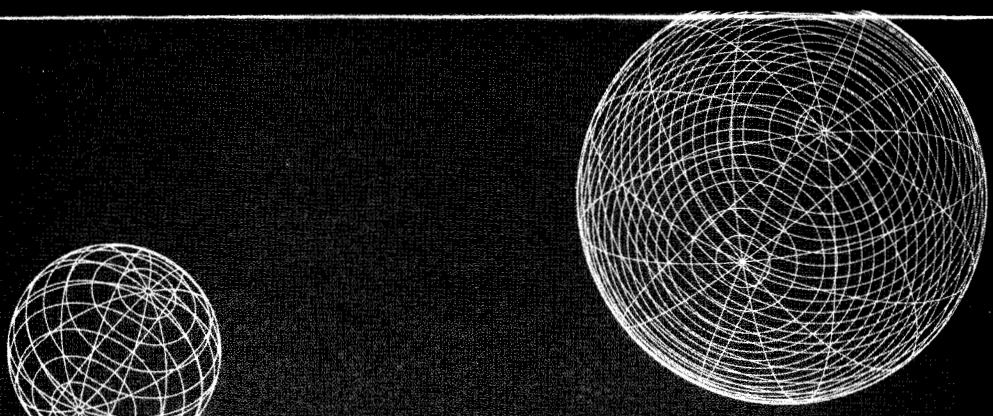

Proceedings of
8 th International Conf

Quantum Communication, Measurement and Computing

Advanced Research
International Conference Center, Tsukuba

Edited by Osamu Hirota,
Jeffrey H. Shapiro and Masahide Sasaki

COHERENT STATE DISTINGUISHABILITY IN CONTINUOUS VARIABLE QUANTUM CRYPTOGRAPHY

Christian Weedbrook[1], Mile Gu[1], Andrew M. Lance[2], Thomas Symul[2], Ping Koy Lam[2] and Timothy C. Ralph[1]

[1]Department of Physics, University of Queensland
St Lucia, Queensland 4072, Australia.
[2]Quantum Optics Group, Department of Physics, Faculty of Science, Australian National University, Canberra, ACT 0200, Australia.

email: weedbrook@physics.uq.edu.au

We use the probability of error as a measure of distinguishability between two pure and two mixed symmetric coherent states in the context of continuous variable quantum cryptography. We show that the two mixed symmetric coherent states (in which the various components have the same real part) never give an eavesdropper more information than two pure coherent states.

1. INTRODUCTION

The security of coherent state continuous variable quantum key distribution (CV-QKD) [1,2] is fundamentally based on the inability of an eavesdropper to perfectly distinguish between non-orthogonal quantum states [3]. In this paper, we look at how much information a potential eavesdropper can gain when trying to distinguish between two pure coherent states as opposed to distinguishing between two mixed coherent states. This is of particular interest in CV-QKD protocols, such as post-selection [2]), where it is important to determine if an eavesdropper obtained more information in the case of distinguishing between pure coherent states or distinguishing between two mixed states.

2. PROBABILITY OF ERROR

In our analysis, we will use the *probability of error* (PE) measure to distinguish between quantum states. We point out that one could potentially consider other distinguishability measures such as the Kolmogorov distance, the Bhattacharyya coefficient and the Shannon distinguishability (for a review of these measures see [4]). However, as we shall see the probability of error measure has a number of useful properties and can be directly calculated for the quantum states we consider in our analysis.

We consider the distinguishability between two general quantum states that are described by the two density matrices $\hat{\rho}_0$ and $\hat{\rho}_1$. It was originally shown by Helstrom [5] that the probability of error between these two density matrices is minimized by performing an optimal positive operator-valued measure (POVM) [3]. In this case, the probability of error for the distinguishing between two general quantum states can be expressed as [4]

$$PE(\hat{\rho}_0, \hat{\rho}_1) = \frac{1}{2} - \frac{1}{4}\sum_{j=1}^{N} |\lambda_j| = \frac{1}{2} - \frac{1}{4}\mathrm{Tr}|\hat{\rho}_0 - \hat{\rho}_1| \tag{1}$$

where $PE(\hat{\rho}_0, \hat{\rho}_1) \in [0, 1/2]$ and λ_j are the eigenvalues of the matrix $\hat{\rho}_0 - \hat{\rho}_1$. We note that when the two states are indistinguishable the probability of error is $PE = 1/2$. On the other hand, in the case when the two states are completely distinguishable the probability of error is $PE = 0$.

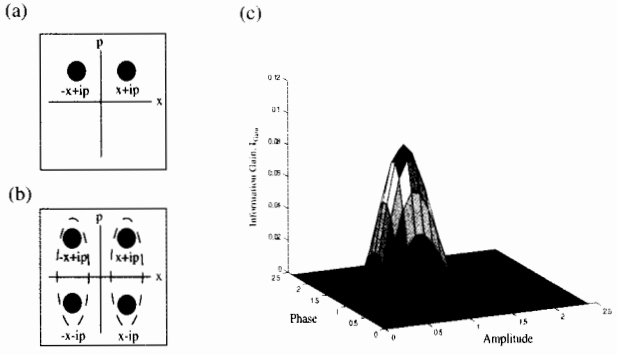

Figure 1: (a) Phase space representation of two pure coherent states and (b) two mixed coherent states. (c) The difference in information rates between the two pure states and two mixed states in terms of the amplitude and phase quadratures, where $I_{gain} = I(\rho_{p_0}, \rho_{p_1}) - I(\rho_{m_0}, \rho_{m_1})$.

3. DISTINGUISHING PURE AND MIXED COHERENT STATES

We now look at distinguishing between two coherent states using the previously defined probability of error. A coherent state is defined as $|\alpha\rangle = \hat{D}|0\rangle$ where $\hat{D} = \exp(\alpha\hat{a}^\dagger - \alpha^*\hat{a})$ is the displacement operator. It is also a minimum uncertainty state and is an eigenstate of the annihilation operator $\hat{a}$, i.e. $\hat{a}|\alpha\rangle = \alpha|\alpha\rangle$ [6], where α is the amplitude of the electromagnetic wave. Any two coherent states $|\alpha\rangle$ and $|\beta\rangle$ are always non-orthogonal and only approach orthogonality (i.e. $\langle\alpha|\beta\rangle \to 0$) when $|\alpha - \beta| \gg 1$ where the magnitude is $|\langle\alpha|\beta\rangle|^2 = \exp(-|\alpha - \beta|^2)$. In the following analysis we will define a coherent state displace in the amplitude and phase quadratures [6], by an amount x and p respectively, as $|\alpha\rangle = |x + ip\rangle$. Consequently, we can write the density operators of two pure coherent states $\hat{\rho}_{p0}$ and $\hat{\rho}_{p1}$ that we consider here as

$$\begin{aligned} \hat{\rho}_{p0} &= |x + ip\rangle\langle x + ip| \\ \hat{\rho}_{p1} &= |-x + ip\rangle\langle -x + ip| \end{aligned} \tag{2}$$

In our analysis we also consider two mixed coherent states, i.e. an equally weighted mixture of coherent states mirrored in the phase quadrature and with both mixtures having the same amplitude component. The density operators corresponding to these two mixed states, $\hat{\rho}_{m0}$ and $\hat{\rho}_{m1}$, are defined as

$$\hat{\rho}_{m0} = \frac{1}{2}(|x + ip\rangle\langle x + ip| + |x - ip\rangle\langle x - ip|) \tag{3}$$

$$\hat{\rho}_{m1} = \frac{1}{2}|-x+ip\rangle\langle -x+ip| + |-x-ip\rangle\langle -x-ip|)$$

Figure (1a) and Fig. (1b) give a two-dimensional phase space illustration of the two pure coherent states and the two mixed coherent states defined by Eq. (2) and Eq. (3) respectively.

According to Eq. (1) we need to determine the eigenvalues of $\hat{A} = \hat{\rho}_0 - \hat{\rho}_1$ for both the two pure states and two mixed states. To do this we write $\hat{A}$ in its matrix representation which can be expanded in terms of the orthogonal Fock or number states $|n\rangle$ defined as [6] $|n\rangle = (\hat{a}^\dagger)^n/\sqrt{n!}|0\rangle$ where $\hat{a}^\dagger$ is the creation operator of a harmonic oscillator and $n \in [0, \infty)$. For example, the coherent state $|x+ip\rangle$ written in terms of this Fock basis is $|x+ip\rangle = \exp[-|\mathrm{x+ip}|^2/2]\sum(\mathrm{x+ip})^n/\sqrt{\mathrm{n!}}|\mathrm{n}\rangle$. Once $\hat{A}$ is written in matrix form we can then numerically determine its eigenvalues. In this Fock state expansion the inner product of an arbitrary coherent state with a Fock state is given by

$$\langle n| \pm x \pm ip\rangle = \frac{(\pm x \pm ip)^n}{\sqrt{n!}}\exp(-\frac{1}{2}(x^2+p^2)) \tag{4}$$

$$\langle \pm x \pm ip|m\rangle = \frac{(\pm x \mp ip)^m}{\sqrt{m!}}\exp(-\frac{1}{2}(x^2+p^2)) \tag{5}$$

where $|n\rangle$ and $|m\rangle$ are Fock states. Calculating the general matrix coefficients for the case of the two pure coherent states we obtain

$$\langle n|A|m\rangle_{pure} = \frac{\exp(-x^2-p^2)}{\sqrt{n!m!}}[(x+ip)^n(x-ip)^m - (-x+ip)^n(-x-ip)^m] \tag{6}$$

Similarly for the two mixed state case we find

$$\begin{aligned}\langle n|A|m\rangle_{mixed} = \frac{\exp(-x^2-p^2)}{2\sqrt{n!m!}}&[(x+ip)^n(x-ip)^m + (x-ip)^n(x+ip)^m \\ &- (-x+ip)^n(-x-ip)^m - (-x-ip)^n(-x+ip)^m]\end{aligned} \tag{7}$$

Numerically we calculate the eigenvalues of Eq. (6) and Eq. (7) up to certain values of n and m. Then according to Eq. (1) this will give us the probability of error in distinguishing between two quantum states. Now having numerically calculated PE we would like to interpret this in terms of the information gained from using the distinguishing measure.

4. SHANNON INFORMATION

In the context of CV-QKD it is important to determine how much Shannon information an eavesdropper can obtain by distinguishing between two (pure or mixed) quantum states. The information obtained by distinguishing between two states can be calculated using the Shannon information formula for a binary symmetric channel [7] $I = 1 + PE\log_2 PE + (1-PE)\log_2(1-PE)$. Figure (1c) shows the difference between the Shannon information obtained by distinguishing between two coherent states $I(\rho_{p_0}, \rho_{p_1})$ compared with distinguishing between two mixed states $I(\rho_{m_0}, \rho_{m_1})$. This information difference is defined as $I_{gain} = I(\rho_{p_0}, \rho_{p_1}) - I(\rho_{m_0}, \rho_{m_1})$. Figure (1c) plots I_{gain} in terms of the amplitude

and phase quadrature displacements of the pure and mixed states defined in Eq. (3) and Eq. (4), respectively. Here we have expanded up to 50 Fock states, i.e. $n = m = 50$.

There are two main features of this plot. Firstly, we notice that, given our distinguishability measure and initial configuration of coherent states in phase space, two mixed states never give more information than two pure states, i.e. $I(\hat{\rho}_{m0}, \hat{\rho}_{m1}) \leq I(\hat{\rho}_{p0}, \hat{\rho}_{p1})$. Secondly, there is a flat region where the information gain is zero, i.e. the information from distinguishing between two mixed states is the same as that of two pure states. This means as we move the states further apart in the amplitude quadrature (while keeping the phase quadrature fixed), the probability of error and information gain both tend to zero. The same result occurs when the amplitude quadrature is fixed while varying the phase quadrature. In this case the states become more mixed when separated leading to a higher entropy. This leads to the two mixed states "behaving" like two pure states, and again, resulting in an information gain of zero.

5. CONCLUSION

In conclusion, we have shown that a CV-QKD protocol where an eavesdropper needs to distinguish between two pure coherent states, rather than two mixed coherent states (where the various mixtures have the same amplitude component), the eavesdropper will never get more information from the two mixed coherent states. We showed this using the probability of error as the distinguishability measure along with the Shannon information formula.

We would like to thank the Australian Research Council for support.

REFERENCES

[1] C. Weedbrook *et al*, Phys. Rev. Lett. **93**, 170504 (2004) (and references therein).

[2] C.Silberhorn *et al*, Phys. Rev. Lett. **89**, 167901 (2002).

[3] M.A. Nielsen and I.L. Chuang, *Quantum Computation and Quantum Information* (Cambridge University Press, 2000).

[4] C.A.Fuchs and J. van de Graaf, IEEE Trans. Info. Theory, **45**, 1216 (1999).

[5] C. W. Helstrom, Quantum Detection and Estimation Theory (Academic, New York, 1976).

[6] C.C.Gerry and P.L.Knight, *Introductory Quantum Optics*, Cambridge, (2005).

[7] C.E. Shannon, Bell Syst. Tech. J. **27**, 623 (1948).

MEASURING PHOTON ANTI-BUNCHING FROM CONTINUOUS VARIABLE SIDEBAND SQUEEZING

Nicolai B. Grosse[1], Thomas Symul[2], Magdalena Stobińska[2], Timothy C. Ralph[3], and Ping Koy Lam[1]

[1]Quantum Optics Group, Department of Physics, Faculty of Science, The Australian National University, ACT 0200, Australia
[2]Instytut Fizyki Teoretycznej, Uniwersytet Warszawski, 00-681 Warszawa, Poland.
[3]Department of Physics, University of Queensland, St Lucia, Australia.

We used a continuous-variable measurement scheme to experimentally probe the second-order temporal coherence $g^{(2)}(\tau)$ of quantum states of light at sidebands to the carrier field. By preparing an appropriately displaced squeezed state, we were able to observe strong photon anti-bunching down to $g^{(2)}(0) = 0.11 \pm 0.18$.

1. INTRODUCTION

For more than fifty years, the Hanbury-Brown Twiss (HBT) interferometer has been used to investigate the second-order coherence of light [1], and to observe photon *anti-bunching* of nonclassical light sources [2–4]. We apply a technique for measuring the second-order coherence $g^{(2)}$ of optical fields, that complements previous studies and provides a link between discrete-variable (DV) and continuous-variable (CV) quantum optics. Our scheme is based on the HBT interferometer, but uses homodyne detection in each arm, to make CV measurements of the quadrature amplitudes over a range of sideband frequencies. At no point is it necessary to make time-resolved detections of single-photons. The $g^{(2)}$ function is constructed from the set of time-averaged correlations between the amplitude/phase quadratures. Homodyne detection offers high bandwidth, and excellent immunity to extraneous optical modes. We used the scheme to measure the temporal second-order coherence $g^{(2)}(\tau)$ of displaced squeezed states, which can exhibit behavior ranging from photon anti-bunching to super-bunching, provided that the state is sufficiently pure, and the squeezing weak. Using our modified HBT interferometer, and exploiting the high stability and low optical loss of our experimental setup, we could prepare and measure displaced squeezed states that clearly demonstrated photon anti-bunching.

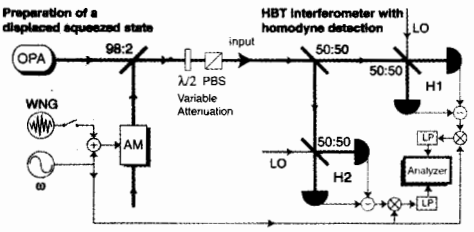

Figure 1: Schematic of the experimental setup.

2. THEORY

The second-order coherence of a single optical mode $\hat{a}$ as measured after the beam-splitter of a HBT inteferometer is

$$g^{(2)}(\tau) = \frac{\langle \hat{b}^\dagger(t+\tau)\hat{b}(t+\tau)\hat{c}^\dagger(t)\hat{c}(t)\rangle}{\langle \hat{b}^\dagger(t)\hat{b}(t)\rangle\langle \hat{c}^\dagger(t)\hat{c}(t)\rangle}, \tag{1}$$

where $\hat{b}=(\hat{a}+\hat{v})/\sqrt{2}$ and $\hat{c}=(\hat{a}-\hat{v})/\sqrt{2}$ with $\hat{v}$ a vacuum mode. Anti-bunching occurs when $g^{(2)}(0)<g^{(2)}(\tau\neq 0)$. The opposite inequality holds true for photon bunching.

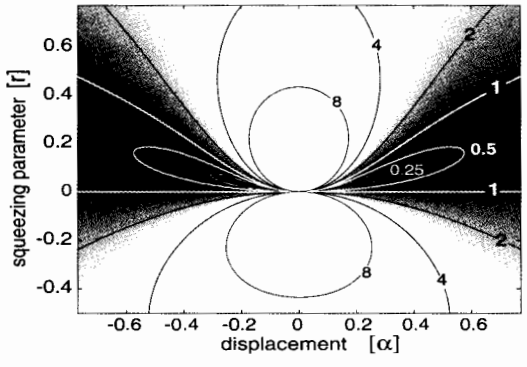

Figure 2: The $g^{(2)}(0)$ parameter space for a displaced squeezed state with squeezing r and displacement α. Regions exhibiting photon anti-bunching are marked progressively darker, with contours giving the precise values.

In the CV regime, we use a pair of homodyne detectors to measure correlations between the field quadratures of amplitude $\hat{X}_a^+ = \hat{a}+\hat{a}^\dagger$, or phase $\hat{X}_a^- = -i(\hat{a}-\hat{a}^\dagger)$. Upon re-expressing Eq. (1) in terms of these we find

$$g^{(2)}(\tau) = \frac{\sum_{i,j}\langle \hat{X}_b^i(t+\tau)^2\hat{X}_c^j(t)^2\rangle - 2\sum_{i,k}\langle \hat{X}_k^i(t)^2\rangle + 4}{(\sum_i\langle \hat{X}_b^i(t)^2\rangle - 2)(\sum_i\langle \hat{X}_c^i(t)^2\rangle - 2)} \tag{2}$$

with $i,j=+,-$ and $k=b,c$. Each correlation or variance term can be measured independently by recording the output of the homodyne detectors, and a value for $g^{(2)}(\tau)$ constructed accordingly. Applying the coherence function Eq. (1) to a weakly squeezed and weakly displaced vacuum state, we transform the operator $\hat{a}$ with $\hat{D}^\dagger(\alpha)\hat{S}^\dagger(r)\hat{a}\hat{S}(r)\hat{D}(\alpha) = \alpha+\hat{a}\cosh r-\hat{a}^\dagger\sinh r$, where $\hat{D}$ and $\hat{S}$ are the unitary displacement and squeezing operators respectively. In an experiment, one selects a particular frequency mode via a filter function, which transforms the operators according to $\hat{a}(\tau)=N^{-\frac{1}{2}}\int_{-\infty}^{\infty}\hat{a}_\omega f(\omega)e^{i\tau\omega}d\omega$ where $f(\omega)$ is the filter and $N=\int_{-\infty}^{\infty}f(\omega)^2d\omega$ for normalization. Choosing $f(|\omega|\leq\Omega)=1$ and zero elsewhere gives the commutation relations $[\hat{a}(0),\hat{a}^\dagger(\tau)] = [\hat{a}(\tau),\hat{a}^\dagger(0)] = \mathrm{sinc}(\Omega\tau)$, which, when applied to Eq. (1), becomes

$$g^{(2)}(\tau) = \frac{1}{\left(\sinh^2(r)+\alpha^2\right)^2}\left\{\left(\alpha^2-\frac{1}{2}\mathrm{sinc}(\Omega\tau)\sinh(2r)\right)^2 + 2\left(1+\mathrm{sinc}(\Omega\tau)\right)\alpha^2\sinh^2(r) + \left(1+\mathrm{sinc}^2(\Omega\tau)\right)\sinh^4(r)\right\}. \tag{3}$$

This function for τ=0 is plotted in Fig. 2 where bunching or anti-bunching statistics can be found with the correct choice of r and α. The stronger cases occur for states approaching the vacuum state $\alpha = r = 0$ for which $g^{(2)}(0)$ is undefined. Eq. (3) is specific to *pure* states, but can be generalized for any Gaussian state having variances $V_{\text{in}}^{+}, V_{\text{in}}^{-}$ and mean α_{in} as measured at the input to the HBT interferometer (see Fig. 1). Although not shown here, this equation was used for making theoretical predictions that were based on the set of measurements $\{V_{\text{in}}^{+}; V_{\text{in}}^{-}; \alpha_{\text{in}}\}$.

3. EXPERIMENT

A schematic is shown in Fig. 1 with: OPA optical parametric amplifier, $\lambda/2$ half-wave plate, PBS polarizing beam-splitter, x:y beamsplitter with transmission x, H1/H2 homodyne detectors, LO local oscillator, AM amplitude modulator, ω function generator, WNG white noise generator, $\otimes$ mixer, LP low pass filter.

Essentially, a displaced squeezed state was prepared from the ouput of a controlled OPA (λ=1064 nm) and weakly interfered with a coherent state. This was sent to the modified HBT interferometer, consisting of two homodyne detectors that measured the correlations between the quadratures amplitudes, which were used to construct $g^{(2)}(\tau)$.

4. RESULTS AND DISCUSSION

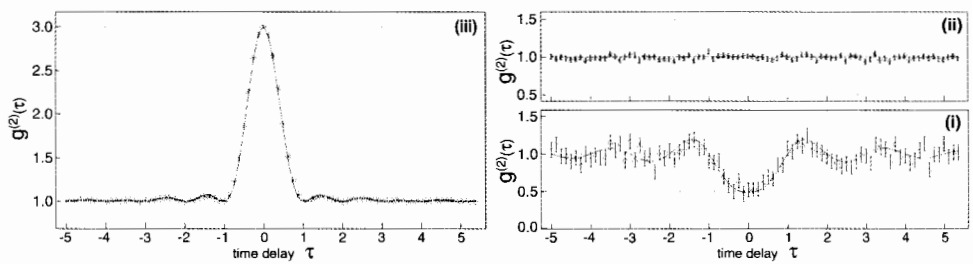

Figure 3: Experimental measurement of $g^{(2)}(\tau)$ with normalized time delay τ in units of bandwidth ($\pi/\Omega = 8.3$ μs). (i) displaced squeezed state, (ii) coherent state, (iii) biased thermal state, curves are theoretical predictions.

Photon anti-bunching statistics from a displaced squeezed state were confirmed by the experimental results. Fig. 3(i) shows how the measured value of $g^{(2)}(0)$ varied as a function of time delay τ. A squeezed state was prepared and measured to have $\{V_{\text{in}}^{+} = 0.902(1); V_{\text{in}}^{-} = 1.137(1)\}$ which was then displaced by $\alpha_{\text{in}} = 0.257(1)$. This state yielded $g^{(2)}(0) = 0.44(22)$ for zero time delay. As τ was increased, $g^{(2)}(\tau)$ approached unity; thereby fulfilling the requirement for photon anti-bunching $g^{(2)}(0) < g^{(2)}(\tau)$.

Shown in Fig. 4(i), displaced squeezed states present their most interesting behavior when $g^{(2)}(0)$ is plotted along a range of displacements. Super-bunching statistics were measured (see inset) from the prepared state $\{V_{\text{in}}^{+}=0.901(3); V_{\text{in}}^{-}=1.136(1); \alpha_{\text{in}}=0.001(2)\}$ which produced $g^{(2)}(0) = 28(10)$. Increasing α_{in} still further, the state found a minimum value corresponding to anti-bunching $g^{(2)}(0) = 0.41(12)$ before approaching one.

Aiming to observe stronger anti-bunching, we prepared a squeezed state having higher purity $\{V_{\text{in}}^{+} V_{\text{in}}^{-} = 0.890(2) \times 1.129(2) = 1.005(3)\}$. The $g^{(2)}(0)$ of this state was measured

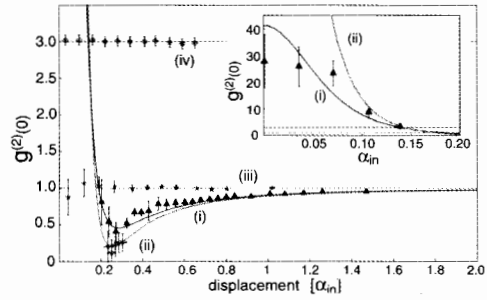

Figure 4: Experimental measurement of $g^{(2)}(0)$ as a function of displacement α_{in}. (i) displaced squeezed state, (ii) weak displaced squeezed state, (iii) coherent state, (iv) biased thermal state, curves are theoretical predictions.

for a range of displacements; Fig. 4(ii). The minimum value occured at $\alpha_{\text{in}} = 0.252(2)$ which yielded $g^{(2)}(0) = 0.11(18)$.

We characterized our HBT interferometer with two test states. A coherent state should produce $g^{(2)}(\tau) = 1$ independent of α_{in}, which was confirmed for $\tau = 0$ in the measurement Fig. 4(iii), and also for variable τ in Fig. 3(ii). We prepared a biased thermal-state $\{V_{\text{in}}^{+} = 14.60(2); V_{\text{in}}^{-} = 1.025(8); \alpha_{\text{in}} = 0.258(1)\}$ and measured $g^{(2)}(0)$ in Fig. 4(iv). This matched the prediction of $g^{(2)}(0) \simeq 3$ for small displacments ($\alpha_{\text{in}} \sim 1$), as did the study for variable τ in Fig.3(iii). The results from both test state measurements agreed with the theoretical predictions, and validated our HBT interferometer.

ACKNOWLEDGMENTS

This work was supported by the Australian Research Council Discovery Grant scheme, and by the MEN Grant No. 1 PO3B 137 30.

REFERENCES

[1] R. Hanbury Brown, and R. Q. Twiss, Nature **177**, 27, (1956).

[2] H. J. Kimble, M. Dagenais, and L. Mandel, Phys. Rev. Lett. **39**, 691 (1977); F. Diedrich and H. Walther, Phys. Rev. Lett. **58**, 203 (1987); G. Leuchs, and U. L. Andersen, Laser Physics **15**, 129 (2005).

[3] J. G. Rarity, P. R. Tapster, and E. Jakeman, Opt. Commun. **62**, 201 (1987); W. A. T. Nogueira, *et al.*, Phys. Rev. Lett. **86**, 4009 (2001); M. Koashi, *et al.*, Phys. Rev. Lett. **71**, 1164 (1993); Y. J. Lu and Z. Y. Ou, Phys. Rev. Lett. **88**, 023601 (2002).

[4] P. Michler, *et al.*, Nature **406**, 968 (2000); C. Santori, *et al.*, Nature **419**, 594 (2002); B. Lounis, and W. E. Moerner, Nature **407**, 491 (2000); B. Darquié, *et al.*, Science **309**, 454 (2005)

SLOWING AND STORING QUANTUM INFORMATION WITH EIT

G. Hétet[1], M. T. L. Hsu[1], O. Glöckl[1], B. C. Buchler[1], J. J. Longdell[2], A. Peng[1], M.T. Johnsson[1], J.J. Hope[1], H.-A. Bachor[1], P. K. Lam[1]

[1]ARC COE for Quantum-Atom Optics, Australian National University, Canberra, ACT 0200, Australia
[2]Laser Physics Centre, RSPhysSE, Australian National University Canberra, ACT 0200, Australia

The properties of Electromagnetically Induced Transparency (EIT) as a mechanism for storing continuous variable information are investigated. Quantum information benchmarks analogous to other quantum information protocols are defined and used to distinguish between quantum and classical memories. We develop an analytical and numerical model of information storage using EIT. In our model we consider the effects of ground state decoherence and the associated atomic quantum noise to identify the experimental parameters required to outperform any classical memory. We also approach the problem experimentally by demonstrating the slowing of modulation sidebands encoded on an optical beam. We demonstrate a reduction of the group velocity of c/30000 of the amplitude and phase quadratures of a continuous wave optical beam using EIT in a thermal rubidium vapor cell and measure the conditional variance of this system.

1. INTRODUCTION

One of the milestones towards quantum computation is a device that allows the storage of quantum information. Following theoretical proposals [1], electromagnetically induced transparency has become the subject of much interest for controlled atomic storage of quantum states of light. Two optical fields, a weak probe and a strong control beam, driving two transitions of a Lambda structure in atoms, set up a extremely narrow transparency window. Associated with this sharp feature is a large decrease of the group velocity of the probe light via steep dispersion. By switching off the control field when the pulse is compressed within the medium, information encoded on the probe remains mapped onto the atomic ground states coherence and can be retrieved by switching the control field back on. Our work aims at quantifying the capabilities of such a scheme for storing continuous variable information.

2. BENCHMARKS

The storage of optical information will be investigated from a quantum informatic perspective. Signal-transfer coefficients T, and conditional variances V_{cv}, have been used in the past as a state independent measure to analyse the effectiveness of teleportation experiments [2,3]. It was shown in Ref . [2] that the quantum regime can be reached with the use of entanglement when $T > 1$ and $V < 1$ simultaneously. We propose to use these quantities to analyze the effectiveness of EIT as a quantum memory.

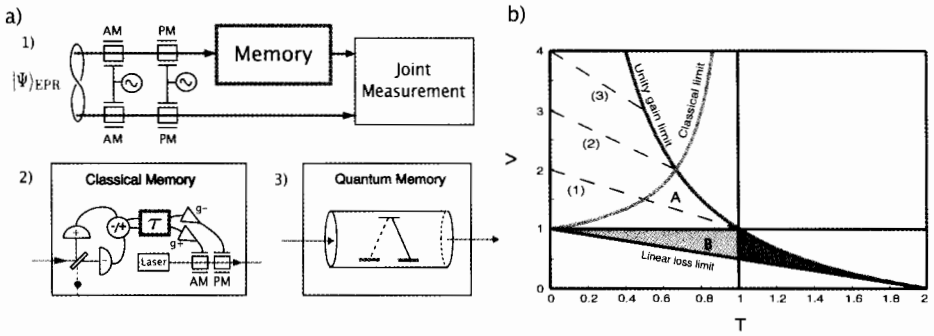

Figure 1: (a) (1) General schematic for characterizing an optical memory. A pair of EPR entangled beams are encoded with amplitude and phase quadrature information. One of these beams is stored and readout from the optical memory whilst the other is being propagated in free space. A joint measurement is then used to measure the quantum correlations between the two beams. (2) A classical teleporter scheme used as an optical memory. (3) Quantum memory using EIT.(b) The TV diagram.

Fig. 1 (a) shows the schematic of our quantum memory benchmark. The efficiency of our EIT quantum memory is compared to the performance of the well known classical teleporter set-up, when used as a quantum memory [2, 4]. The conditional variances and signal transfer coefficients are defined respectively as

$$V_{\rm cv}^{\pm} = V_{\rm out}^{\pm} - \frac{|\langle \hat{X}_{\rm in}^{\pm} \hat{X}_{\rm out}^{\pm} \rangle|^2}{V_{\rm in}^{\pm}} \text{ and } \mathrm{T}^{\pm} = \frac{\mathcal{R}_{\rm out}^{\pm}}{\mathcal{R}_{\rm in}^{\pm}} \tag{1}$$

where $\mathcal{R}_{\rm out/in}^{\pm}$ is the signal-to-noise ratio of the output/input field. The performances of the system on both conjugate observables is evaluated using V and T defined respectively by

$$V = \sqrt{V_{\rm cv}^{+} V_{\rm cv}^{-}} \text{ and } \mathrm{T} = \mathrm{T}^{+} + \mathrm{T}^{-} \tag{2}$$

Fig. 1(b) shows the plot of a TV-diagram. A classical memory cannot overcome the $T > 1$ or $V < 1$ limits. By tuning the feedfoward gain, g, a classical memory will in fact perform at best at the "classical limit" curve. With quantum resources such as entanglement or with the use of a quantum memory both $T > 1$ and $V < 1$ limits can be overcome, and the protocol can perform in region (C), corresponding to the quantum regime.

When a quantum memory system does not generate excess noise, its performance is described by the linear loss limit line. The evolution of T and V as a function of the linear loss and possible excess noise introduced by the memory is also plotted. The linear loss line and the dotted lines (1) to (3) describe the TV performance with varying transmittivities where each of the lines differs to the previous by one quantum of excess noise.

3. MODELING OF QUANTUM INFORMATION STORAGE WITH EIT

We perform numerical simulations to determine whether EIT can store continuous variable information better than the quantum limit. The atomic structure is approximated by a 3-level Lambda system, where the two ground states are degenerate.

We consider the simultaneous storage of both quadratures of the probe field when amplitude and phase modulations are encoded within the EIT bandwidth and evaluate the amount of loss and excess noise on the output field using stochastic simulations in the positive-P representation [5] of the field. The probe beam is treated as a general quantized field with longitudinal spatial dependence z, and the coupling beam as a classical field. Decoherence terms are also introduced to account for elastic and non-elastic collisions.

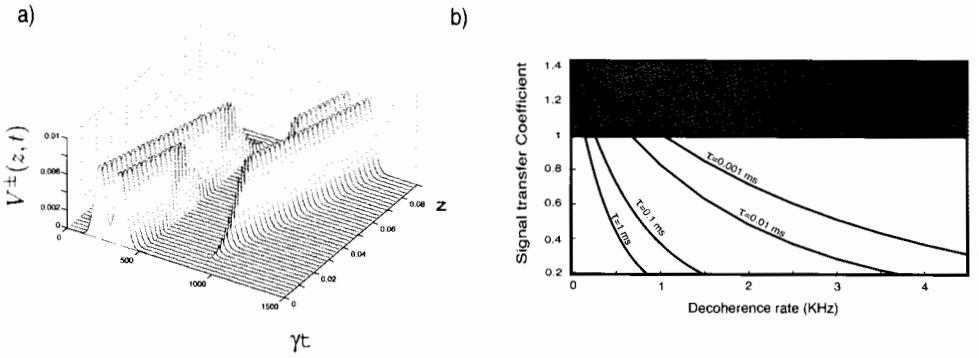

Figure 2: (a) Stochastic simulations showing the storage of the amplitude quadrature of a modulated pulse. (b) Total signal transfer coefficient T as a function of the decoherence rate for storage times $\tau = 1, 0.1, 0.01, 0.001$ ms in the linear loss regime. For τ=1, 0.1, 0.01, 0.001 ms the quantum memory requires γ_0<0.33, 0.5, 0.7, 1.1 kHz respectively. We used numbers from the ^{87}Rb line.

Fig. 2 (a) shows the results of this simulation showing the propagation of the amplitude quadrature of the modulated pulse through the cell. The calculation of the variance of the output field reveals that only 25 % of the signal is absorbed with small amounts of excess noise introduced in the storage process.

A simple analytical treatment of light storage using EIT shows a good agreement with this model. When the control field is turned off and on abruptly, an exact analytical expression of the losses in the medium in the presence of elastic collisions can be found. This allows to graph the evolution of the signal transfer coefficient T as a function of the decoherence rate (Fig. 2 (b)). Under small decoherence values, our result shows that EIT can be used to store continuous variable information better than the quantum limit defined by T = 1.

4. CONDITIONAL VARIANCE MEASURE OF EIT AS A DELAY LINE

The noise performance of EIT as a quantum delay line for continuous variables is experimentally analyzed [6]. A delay of c/30000 was measured for both quadratures of the field. The conditional variance between the input and output beams is then evaluated as described in Fig. (3) (a). The subtracted signal between the input and output is minimized with variable gain $G(\omega)$ and time delay $\tau(\omega)$. The results are shown Fig. 3(b). The $V_{cv}^{\pm}(\omega)$ found using a beamsplitter to simulate the passive loss of the EIT system are the datasets labelled (ii). EIT data (i) is well above the passive loss benchmark (ii), showing that excess noise is added to the delayed probe beam. For certain frequencies however, correlations are preserved better than any classical delay line with a conditional variance dropping below 1. The no-cloning limit was however not overcome due to the excess noise at low frequencies, where the linear losses are smaller.

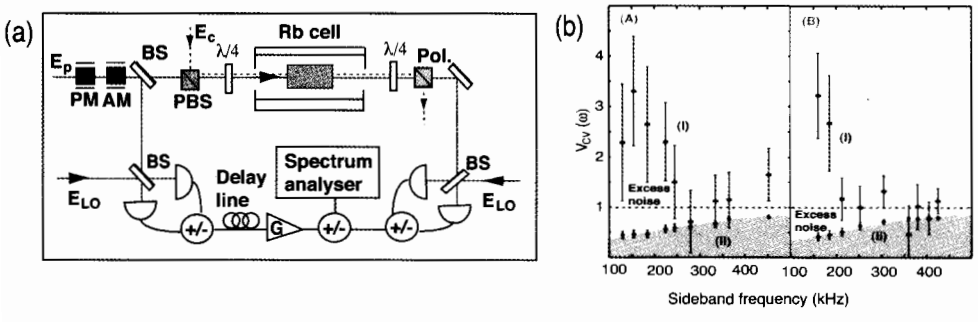

Figure 3: (a) Schematic of the experiment used to measure the conditional variance CV. (b) CV measurements for the two quadratures. (A) Amplitude quadrature; (B) phase quadrature. The data point groups represent the (i) EIT CV and (ii) beam-splitter benchmark CV. The output homodyne locking error is responsible for the error bars.

REFERENCES

[1] M. Fleischhauer and M. D. Lukin, Phys. Rev. Lett. **84**, 5094 (2000).

[2] T. C. Ralph and P. K. Lam Phys. Rev. Lett. **81**, 5668 (1998).

[3] W. P. Bowen, N. Treps, B. C. Buchler, R. Schnabel, T. C. Ralph, Hans-A. Bachor, T. Symul, and P. K. Lam. Phys. Rev. A **67** 032302 (2003).

[4] K. Hammerer, M. M. Wolf, E. S. Polzik, and J. I. Cirac Phys. Rev. Lett. **94**, 150503 (2005).

[5] P. D. Drummond and C. W. Gardiner J. Phys. A **13**, 2353 (1980).

[6] M.T.L. Hsu, G. Hétet, O. Glöckl, J. J. Longdell, B. C. Buchler, H.-A. Bachor, P. K. Lam Phys. Rev. Lett. **97**, 183601 (2006)

9784904020005

ISBN978-4-904020-00-5

NiCT National Institute of Information and Communications Technology

ICT Value Chain